Analyst

PAPER

View Article Online
View Journal | View Issue

Cite this: *Analyst*, 2025, **150**, 4972

Two-dimensional correlation spectroscopy (2D-COS) in the analysis of parasitemia in Raman spectra of red blood cells of patients diagnosed with malaria

Mateusz Migdalski, [a] Jacek Czepiel, [b,c] Paulina Moskal, [a] Malwina Birczyńska-Zych, [b,c] Martyna Kucharska, [a] Grażyna Biesiada, [b,c] Joanna Stokłosa,[a] Monika Bociąga-Jasik [b,c] and Aleksandra Wesełucha-Birczyńska *[a]

This study focused on finding correlations between Raman bands present in patients infected with *Plasmodium falciparum* (*P. falciparum*) malaria at different levels of parasitemia (parasite concentrations in blood). The obtained spectra were analysed using two-dimensional correlation spectroscopy (2D-COS) to find out how the Raman bands correlate with each other depending on the level of parasitemia in the patients. A laser line with a wavelength of 442 nm was used to excite the heme resonance, which allowed for obtaining enhanced bands in the heme vibration spectrum. Synchronous auto-peaks were found to be generated by marker vibrations of ν_4 and ν_{37} deoxy-heme structures at position 1354 cm^{-1} and 1580 cm^{-1}, respectively. The observed cross-peaks were caused by vibrations of deoxyheme structures, often characteristic of hemozoin. For the normal Raman effect, a laser line with a wavelength of 785 nm was used, which allowed obtaining additional information about the structure of infected erythrocytes and enabled the detection of many changes in the structure of proteins and lipids of red blood cells, while the resonance Raman effect focused almost exclusively on changes in the heme structure. Therefore, two-dimensional maps created from these results differed significantly, indicating different spectral regions depending on the laser line used. And thus, many auto-peaks appear for the 785 nm excitation line, which, in addition to the peaks characteristic for heme, also originate from amino acids, protein and lipid structures. Different positions of asynchronous cross-peaks come from different intermediates that characterize the oscillations of ν_4 heme structures. Both synchronous and asynchronous 2D correlation maps for laser lines 442 nm and 785 nm, respectively, allow not only to notice changes in the intensities of correlated band, but also phase shifts between bands – *i.e.* the order of changes occurring between correlated Raman bands. It was observed that 442 nm excitation laser line created conditions for observing specific heme intermediates. The potential possibility of using the relative Raman intensity of the bands representing the oxy- and deoxy-heme structure, I_{1370}/I_{1354}, to correlate with the levels of malarial parasitemia observed in blood samples is discussed.

Received 7th March 2025,
Accepted 6th October 2025

DOI: 10.1039/d5an00272a

rsc.li/analyst

Introduction

Despite constant advancements in medicine, malaria is still a dangerous and potentially deadly infectious disease. Globally in 2024, there were nearly 250 million estimated malaria cases, of which over 600 thousand proved fatal, especially in the WHO Africa Region, which accounted for nearly 94% of cases globally.[1] Out of five *Plasmodium* species *Plasmodium falciparum* (*P. falciparum*) is the deadliest malaria parasite, as well as the most prevalent on the African continent. If left untreated, *P. falciparum* malaria can progress to a severe form of the disease and lead to death within 24 hours of the first symptoms appearing.[2] Mild symptoms include fever, chills, headache, or muscle aches, while serious symptoms may include fatigue, confusion, seizures, and breathing difficulty.[2,3] In the endemic malaria regions with limited access to clinical care, laboratory-based diagnosis may be

[a]*Faculty of Chemistry, Jagiellonian University, Gronostajowa 2, 30-387 Kraków, Poland. E-mail: birczyns@chemia.uj.edu.pl; Tel: +48 126862772*
[b]*Department of Infectious Diseases, Jagiellonian University, Jakubowskiego 2, 30-688 Kraków, Poland*
[c]*Department of Infectious Diseases, The University Hospital in Kraków, Jakubowskiego 2, 30-688 Kraków, Poland*

difficult to obtain, if at all possible. Therefore, rapid diagnostic tests (RDTs) may be the only form of easily accessible diagnostic tool.[4] These tests utilise the principles of chromatography, combined with antibodies targeting a specific antigen present in *Plasmodium* parasites.[4] Histidine-rich protein 2 (HRP2) is a protein produced by *P. falciparum* parasite, which is closely associated with the development of the parasite.[5] This protein is used in RDTs to detect malaria caused by *P. falciparum*. Certain parasites however may not express HRP2 protein, resulting in a falsely negative result of an RDT. At high parasite densities (high parasitemia) histidine-rich protein 3 (HRP3), a homologue protein of HRP2, may cross-react with monoclonal antibodies used for malaria detection. With lower parasitemia levels or if the parasite expresses neither HRP2 nor HRP3, *P. falciparum* will completely evade detection with RDTs.[1] This phenomenon presents a challenge for current diagnostic methods, which prompts the creation of new techniques, capable of diagnosing *P. falciparum* malaria regardless of HRP2 and HRP3 expression or parasitemia levels.

In our previous papers,[6–9] we have proven, that detecting *P. falciparum* infection in red blood cells (RBCs) found in blood samples from patients diagnosed with malaria is possible using Raman spectroscopy (RS), and especially resonance Raman (RRS) spectroscopy. We also checked the usefulness of 2D correlation spectroscopy, to indicate the specificity of aging between healthy and *P. falciparum*-infected erythrocytes.[10] It also turned out that the 2D-COS method allows to distinguish the activity of different *Plasmodium* parasites on erythrocytes.[11]

In this work, averaged Raman spectra from blood samples differing in parasitemia levels were compared using two-dimensional correlation spectroscopy (2D-COS) to resolve how different parasitemia levels affect the obtained spectra and how they are related to each other.

Experimental

Blood samples

Blood samples were provided from patients diagnosed with *P. falciparum* malaria in cooperation with the Jagiellonian University Hospitals Department of Infectious and Tropical Diseases. These samples were transported to the laboratory at the Faculty of Chemistry of the Jagiellonian University immediately after collection. Blood smears had been performed on a microscope slide, after which an isolated RBC had been selected under a microscope and probed using RS and RRS techniques.

In order to make a final diagnosis of malaria and determine the level of parasitemia, optical microscopic identification of a blood smear with Giemsa staining was performed by qualified personnel in the Laboratory of Parasitology of the University Hospital in Kraków. The parasitemia level in analysed blood samples ranged from 0.09% to 11.3%.

This study was carried out in accordance with the guidelines for good clinical practice (GCP), in accordance with the principles of ethics of medical research, involving people as defined by the Helsinki Declaration. All studies were approved by the Bioethics Committee of the Jagiellonian University. Informed consent was obtained from all patients involved in the study.

Spectral measurements

For Raman measurements Renishaw InVia and Renishaw InVia Qontor spectrometers had been used. For light excitation source KIMMONs He–Cd and diode HPNIR lasers were used, generating 442 nm and 785 nm laser lines, respectively.

Obtained Raman spectra were preliminary pre-processed using WiRE v.3.4 software, in order to reduce noise, subtract background and remove spikes caused by cosmic rays if necessary.

For each patient, 2–4 red blood cells were measured using the mapping technique. At a wavelength of 442 nm, 20, 26, 22, 20, 20 and 15 spectra were measured for parasitemia levels of 11.3%, 7.45%, 1.17%, 0.16%, 0.14%, 0.09%, respectively (Fig. 1A). At the wavelength of 785 nm, 26, 17, 20 and 15 spectra were measured for the parasitism level of 7.45%, 1.17%, 0.16%, 0.09%, respectively (Fig. 1B). The obtained spectra were averaged for each patient, which allowed for grouping the spectra based on the level of parasitemia. Generalized 2D-COS was performed.[12–14] The 2D correlation maps were created and analyzed using the SpectraCorr 1.1 Omnic 9 software. The mathematical foundations of 2D spectroscopy used in the software is contained in several articles.[12,15,16] The reference spectrum was taken as equal to zero, therefore the dynamic spectra were identical to the observed changes in spectral intensity. The parasitemia level was regarded as an external perturbation. The averaged spectra for the 442 nm and 785 nm laser lines, with highlighted Raman bands, used in 2D-COS analysis are shown in Fig. 1. Each of the spectra used to generate two-dimensional spectra is the average obtained for a given parasitemia level.

Results & discussion

Raman spectroscopy

An enhancement of the Raman spectrum characteristic for heme was observed when the excitation line was shorter than 500 nm.[16] Heme is the dominant component of red blood cells.[7] The most distinct Raman band in the range of 1350–1380 cm^{-1} corresponds to the totally symmetric ν_4 vibrational mode and represents in-plane porphyrin ring vibrations, ν(pyr half-ring), of A_{1g} symmetry.[17] By observing the ν_4 band at 442 nm excitation, an interesting dependence on the degree of parasitemia was observed (see Fig. 1A). The spectral range of 1380–1340 cm^{-1} indicates the presence of two clearly different heme structures, around 1354 cm^{-1} deoxy- and around 1370 cm^{-1} oxy-heme structure.[18,19] The position of these peaks was determined from the spectrum corresponding to the lowest parasitemia level (see Fig. 2A, bottom). However, band around 1350 cm^{-1} is not a pure band. In addition to the ν_4 band characterizing the two structures of heme, oxy- and deoxy-, one may expect ν_{21} band at *ca.* 1307 cm^{-1} of A_{2g} symmetry (δ C_mH), ν_{41} band at *ca.* 1340 cm^{-1}

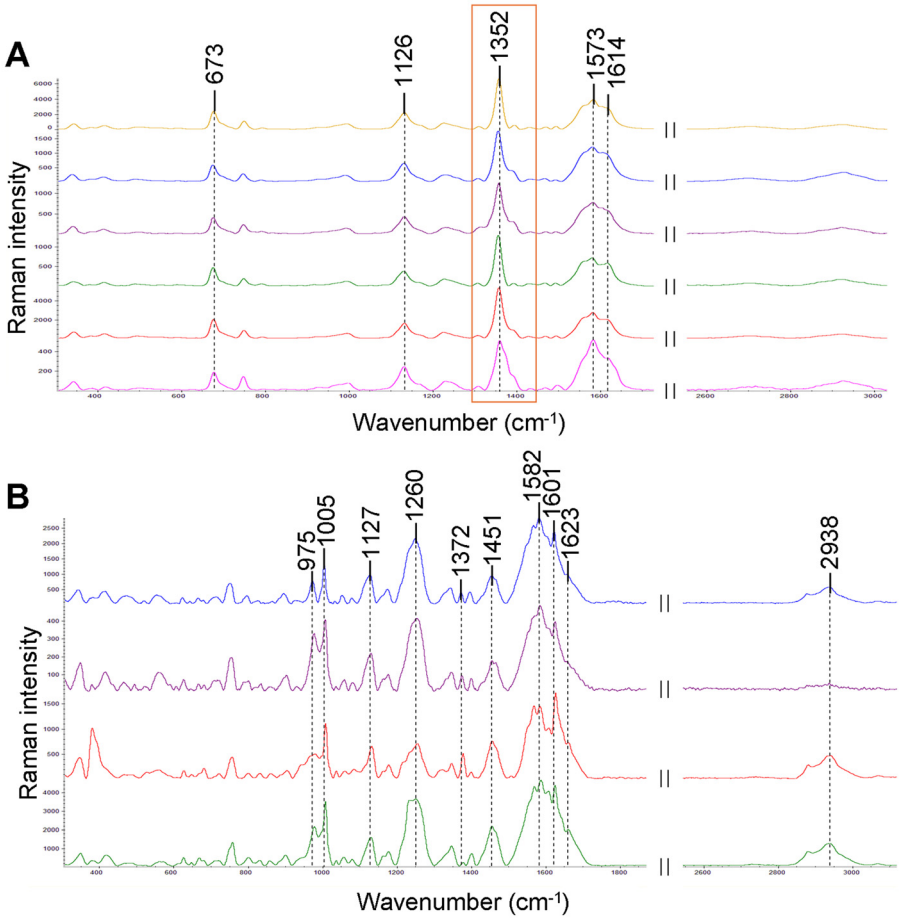

Fig. 1 Averaged Raman spectra differing in parasitemia in blood samples. (A) Results obtained using 442 nm laser line (the resonance-enhanced ν_4 band is marked). (B) Results obtained using 785 nm laser line.

of E_u symmetry (ν(pyrrole half-ring)$_{sym}$), and ν_{29} band at *ca.* 1399 cm^{-1} of B_{2g} symmetry (ν(pyrrole quarter-ring)$_{sym}$) (according to Spiro[16] and Wood & McNaughton[20]).

The structure of deoxy-heme characterizes *Plasmodium* infected erythrocytes.[8,10,20]

Relative intensities of the ν_4 I_{1370}/I_{1354} band (see Fig. 2B) were obtained from curve fit (red line *vide* Fig. 2A), and additionally obtained from intensity reading at position 1370 cm^{-1} and 1354 cm^{-1} (black line). The latter method is simpler to implement and can potentially be considered for rapid diagnostic applications.

The relative intensities of the Raman bands representing the oxy- and deoxy-heme structure correspond to the degree of parasitemia observed in blood samples taken from patients hospitalized due to *P. falciparum* malaria (see Fig. 2B). This opens up an interesting possibility of rapid assessment of the degree of parasitemia based on the intensity of the bands characterizing the ν_4 vibration. It seems that it may be a helpful tool to determine parasitemia at low-levels, lower than 2%. This potential possibility needs to be thoroughly verified as red blood cells infected in other ways also have similar characteristics.[21–24] Therefore, confirmation of this possibility requires building a sufficiently large database.

The spectra in the case of different degrees of parasitemia, apart from the mentioned marker band ν_4, are actually quite similar, hence the idea of using two-dimensional correlation (2D-COS) to unravel hidden dependencies and gain new knowledge.

Raman spectra obtained at 785 nm excitation provide information not only about the structure of heme but also about proteins and the erythrocyte membrane (see Fig. 1B and Table 1). More bands appear in the spectrum than in the case of resonance, the intensity of which is proportional to the square of the change in polarizability.

2D correlation spectroscopy

Two- dimensional correlation spectroscopy (2D-COS) is a technique which allows for the analysis of changes in the intensity of vibrations induced by external perturbation, observed in a specific range of an external variable. Therefore, 2D correlation intensity $X(\nu_1,\nu_2)$ is a measure of the comparison of the spectral intensity changes measured for two spectral variables ν_1 and ν_2 for a given external variable, so it allows to obtain additional aspects of a studied dataset.[12,13] In this approach two orthogonal axis of independent spectral variables define the 2D spectral plane, while the third axis defines the spectral

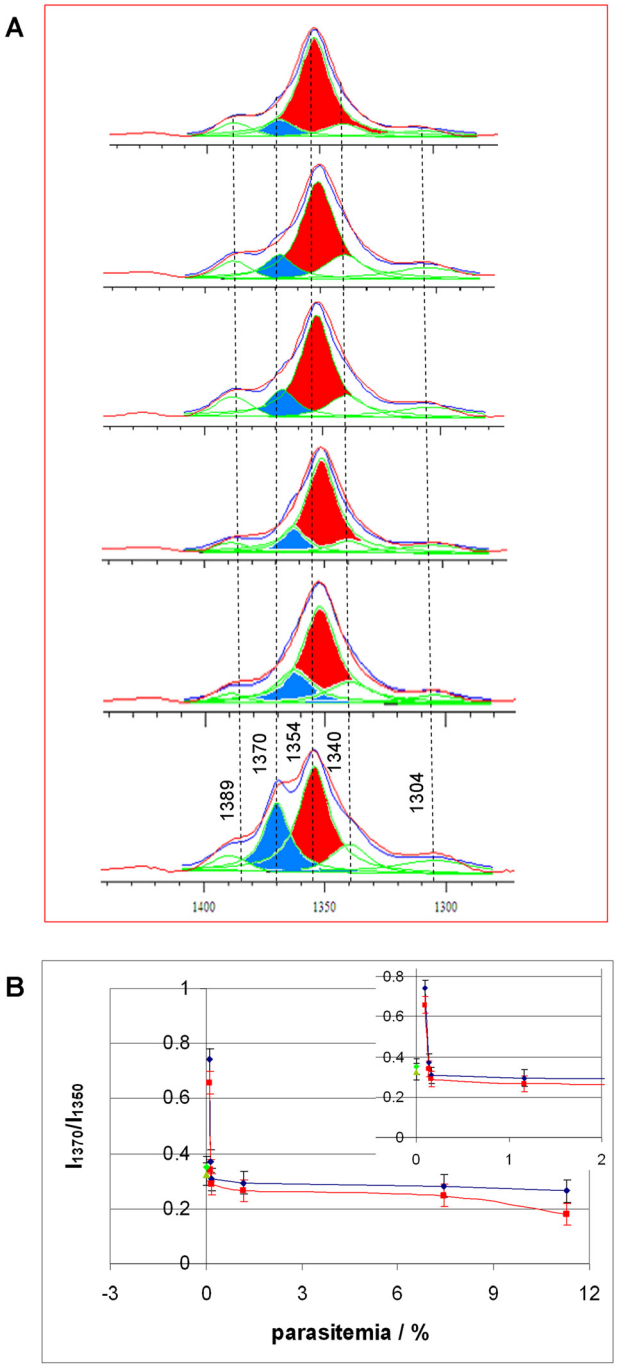

Fig. 2 (A) Decomposition of the ν_4 resonance-enhanced band for different degrees of parasitemia; the oxy-heme component is marked in blue and the deoxy-heme component in red; (B) relative intensities of the ν_4 I_{1370}/I_{1354} band representing oxy-heme and deoxy-heme structures, respectively, as a function of parasitemia dependence obtained from curve fit (*vide* A, red line), and obtained from intensity reading at position 1370 cm^{-1} and 1354 cm^{-1} – black line. The intensity ratio value of I_{1370}/I_{1354} for healthy red blood cells is marked with a green triangle (from curve fit) and a green diamond (directly from the averaged spectrum).

Table 1 Observed Raman bands and their assignments for malaria infected RBCs excited with 442 nm and 785 nm laser line[6–10,20,30,33]

Raman band position [cm^{-1}]		
442 nm	785 nm	Assignments
673		Heme; ν_7 (deoxy)
	975	Heme; ν_{46} (deoxy); backbone Skeletal vibrations; proteins; lipids
	1005	Heme (Hz); ν_{45}; Phe
1126	1127	Heme; ν_{22}; Asp, Glu, Thr; ν(C–C), *trans* lipid conformation
	1260	Amide III, ν(C–N), δ(N–H), ν(C═O), δ(O═C–N)
1352		Heme; ν_4 (deoxy); Trp
	1372	Heme; ν_4 (oxy); Trp; PC, $\omega(CH_2)$
	1451	$\delta(CH_2/CH_3)$
1573	1582	Heme (Hz); ν_2, Asp, His
	1601	ν(C–C)
1614	1623	Tyr
	2938	$\nu(CH_3)_{sym}$, PE, proteins and Lipids

Heme vibration notation based on calculations from ref. 19. Asp – aspartic acid, Glu – glutamic acid, His – histidine, Hz – hemozoin, Phe – Phenylalanine, Thr – threonine, Trp – tryptophan, Tyr – tyrosine, PC – phosphatidylcholine.

intensity caused by an external perturbation. $X(\nu_1,\nu_2)$ can be treated as a function of complex numbers consisting of two orthogonal components: synchronous and asynchronous.[14]

$$X(\nu_1,\nu_2) = \Phi(\nu_1,\nu_2) + {}_i\Psi(\nu_1,\nu_2).$$

2D intensity synchronous correlation $\Phi(\nu_1,\nu_2)$ shows the similarity or coincidence trends between two separate intensity changes measured at different spectral variables when the parameter is scanned over a fixed range. Asynchronous 2D intensity correlation $\Psi(\nu_1,\nu_2)$ indicates dissimilarity or out-of-phase dependencies between intensity changes.

Results obtained with a 442 nm laser line

Synchronous 2D map obtained using 442 nm laser line (see Fig. S1 and Fig. 3A) showed two prominent autopeaks, visible at 1352 cm^{-1} and 1580 cm^{-1}.[8,17,20,25,26] Bands related with those peaks are associated with symmetric stretching of deoxy-heme ν_4 (ν_{sym}(pyr. half-ring)) and antisymmetric stretching mode ν_{37} of deoxy-heme ($\nu_{asym}(C_\alpha–C_m)$), respectively. In addition to the above-mentioned autopeaks, several distinct, positive cross-peaks can also be observed.

The first two cross-peaks result from the correlation of the symmetric stretching vibration of the pyrrole half-ring of deoxy-heme ν_4 (ν_{sym}(pyr. half-ring)) around 1350 cm^{-1} with the ν_7 symmetric deformations of the pyrrole ring of deoxy-heme (δ_{sym}(pyr. deform)) at 673 cm^{-1} and also with 1126 cm^{-1} vibration due to ν_{22} the pyrrole half-ring antisymmetric stretching (ν_{asym}(pyr. half-ring)). The next two cross-peaks come from the correlation of the symmetric stretching mode ν_2 of deoxy-heme $\nu_{sym}(C_\beta–C_\beta)$ at wavenumber of 1576 cm^{-1} with 673 cm^{-1} due to ν_7 deoxy-heme δ_{sym}(pyr. deform.) and also with 1126 cm^{-1} due to ν_{22} of the pyrrole half-ring (ν_{asym}(pyr. half-ring)).[20,27]

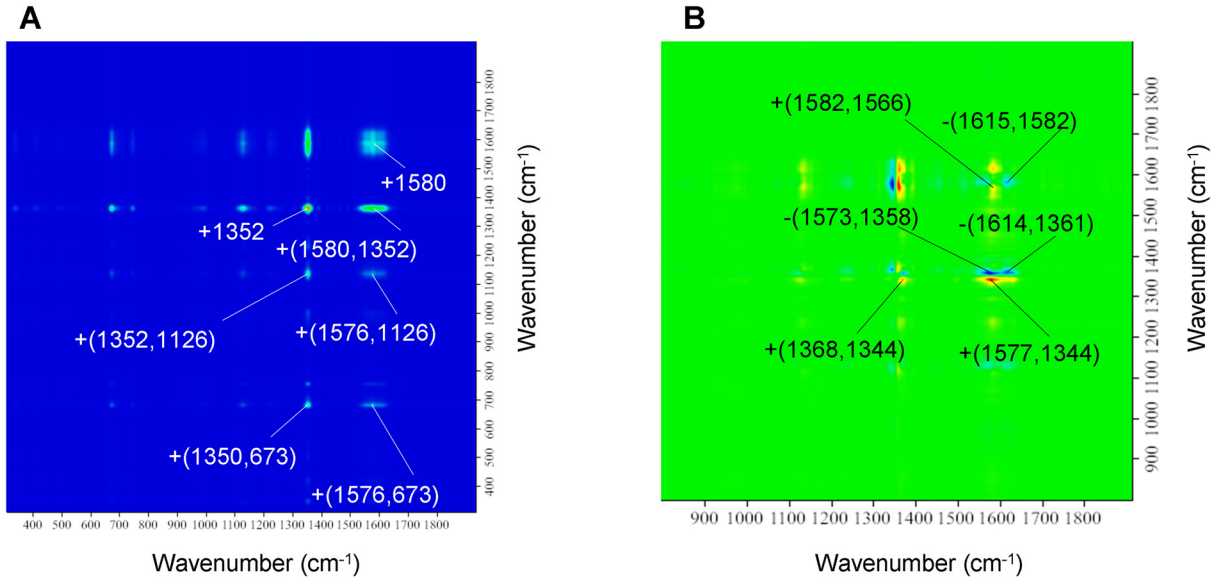

Fig. 3 2D map (*vide* Fig. S1)(A) synchronous in the spectral range 1900–300 cm^{-1}, and (B) asynchronous in the spectral range 1900–800 cm^{-1} obtained by correlating Raman spectra obtained using 442 nm laser line. The peaks of interest are labelled.

Finally, the cross-peak at +(1580, 1352) cm^{-1} shows the correlation between antisymmetric stretching mode ν_{37} of deoxy-heme ($\nu_{asym}(C_\alpha–C_m)$) and ν_4 symmetric stretching of deoxy-heme (ν_{sym}(pyr. half-ring)).[20,26,27]

Synchronous cross-peaks are generated mainly as a result of changes in the deoxy-heme structures.[20,27]

Asynchronous 2D map created by using spectra obtained with a 442 nm laser line contains many prominent cross-peaks, present in the characteristic spectral heme region (see Fig. 3B).[8,10,20] Cross-peak at +(1368, 1344) comes from bands corresponding to the (ν_4) symmetric stretching mode of oxy-heme (ν_{sym}(pyr. half-ring)) and (ν_{41}) symmetric stretching mode of deoxy-heme (ν_{sym}(pyr. half-ring)). Cross-peak at −(1573, 1358) originates from bands indicating deoxy-heme (ν_2) stretching mode of two C_β carbons ($\nu(C_\beta–C_\beta)$) and (ν_4) symmetric stretching mode of deoxy-heme (ν_{sym}(pyr. half-ring)). Cross-peak at +(1577, 1344) subsists of bands correlating (ν_2) and (ν_{41}) symmetric stretching mode of oxy-heme (ν_{sym}(pyr. half-ring)). The +(1582, 1566) cross-peak represents a correlation between (ν_{37}) antisymmetric stretching of deoxy-heme ($\nu_{asym}(C_\alpha–C_m)$) and (ν_2) an oxy-heme stretching mode of two C_β carbons ($\nu(C_\beta–C_\beta)$).

Tyr vibrations around 1615 cm^{-1} correlate negatively with two marker vibrations of heme 1361 cm^{-1} (ν_4) and 1582 cm^{-1}(ν_{37}), which means that they precede changes in the amino acid.

Asynchronous cross-peaks are generated mainly as a result of changes in deoxy-heme structures, which also generate the changes observed in oxy-heme structures, certain amino acids, such as Trp and/or Tyr.[20,26–28] Trp, Tyr and His are amino acids whose presence indicates the appearance of the parasitic protein HRP2.[11,29,30]

All cross-peaks visible in the two-dimensional synchronous and asynchronous correlation map generated using spectral data acquired with a 442 nm laser line are summarized in Table 2.

The two-trace two-dimensional (2T2D) correlation spectroscopy technique was also used to find the specificity of the averaged Raman spectrum for a given level of parasitemia compared to the averaged spectrum of healthy volunteers.[31] The resulting asynchronous maps are shown in the Fig. 4. Asynchronous spectrum provides much more discriminating information. Cross-peaks in the asynchronous 2T2D spectrum indicate that the two bands corresponding to the spectral coordinate that have different sources. For the parasitemia level of 0.09% cross-peak +(1349,1369) indicates that the intensity of the deoxy-heme structure is in the reference spectrum of a healthy blood cell is more abundantly represented than that of oxy-heme in the sample spectrum. The next prominent cross-peak +(1347,1579) indicates that the intensity of the deoxy-structure is in the reference spectrum of the healthy blood cell in higher abundance than the band ν_2 ($\nu(C_\beta–C_\beta)$) in the sample spectrum. Similar cross-peaks appear for the parasitemia level of 0.14%, positive at coordinates +(1344, 1356) (ν_{41}, ν(pyrrole half-ring)$_{sym}$ and ν_4, deoxy), and, but now negative, at 1356 cm^{-1} (ν_4 (deoxy)), correlating with 1568 cm^{-1} (ν_2, Hz, $\nu_{sym}(C_\beta–C_\beta)_{oxy}$) and with 1594 cm^{-1} (ν(C–C), Tyr). These negative cross-peaks indicate the predominance of the functional group represented by the second coordinates in the healthy blood cell sample.

For subsequent levels of parasitemia the asynchronous maps are similar (Fig. 4C–F). Cross-peaks coordinates indicate important functional groups that are changed during the *Plasmodium* infection process. Differences related to the band

Table 2 The prominent synchronous and asynchronous cross-peaks and their assignments, 442 nm laser line[11,16–20,27–28,30]

Synchronous				Asynchronous		
Auto-peaks	Assignments			Assignments	Cross-peaks	Assignments
1352	ν_4, ν_{sym}(pyr. half-ring)$_{deoxy}$			ν_4, ν_{sym}(pyr. half-ring)$_{oxy}$	+(1368, 1344)	ν_{41}, ν_{sym}(pyr. half-ring)$_{deoxy}$
1580	ν_{37}, ν_{asym}(C_α–C_m)$_{deoxy}$			ν_2, Hz, ν_{sym}(C_β–C_β)$_{deoxy}$, Asp, His	−(1573, 1358)	ν_4, ν_{sym}(pyr. half-ring)$_{deoxy}$
Assignments	Cross-peaks	Assignments		ν_2, Hz, ν_{sym}(C_β–C_β)$_{deoxy}$	+(1577, 1344)	ν_{41}, ν_{sym}(pyr. half-ring)$_{deoxy}$
ν_4, ν_{sym}(pyr. half-ring)$_{deoxy}$	+(1350, 673)	ν_7, δ_{sym}(pyr. deform)$_{deoxy}$		ν_{37}, ν_{asym}(C_α–C_m)$_{deoxy}$Tyr	+(1582, 1566)	ν_2, Hz, ν_{sym}(C_β–C_β)$_{oxy}$
	+(1352, 1126)	ν_{22}, Hz, ν_{asym}(pyr. half-ring)			−(1614, 1361)	ν_4, ν_{sym}(pyr. half-ring)$_{deoxy}$
ν_2, Hz, ν_{sym}(C_β–C_β)$_{deoxy}$	+(1576, 673)	ν_7, δ_{sym}(pyr. deform)$_{deoxy}$			−(1615, 1582)	ν_{37}, ν_{asym}(C_α–C_m)$_{deoxy}$
	+(1576, 1126)	ν_{22}, Hz, ν_{asym}(pyr. half-ring)				
ν_{37}, ν_{asym}(C_α–C_m)$_{deoxy}$	+(1580, 1352)	ν_4, ν_{sym}(pyr. half-ring)$_{deoxy}$				

Hz – hemozoin, Asp – aspartic acid, His – histidine, Tyr – tyrosine.

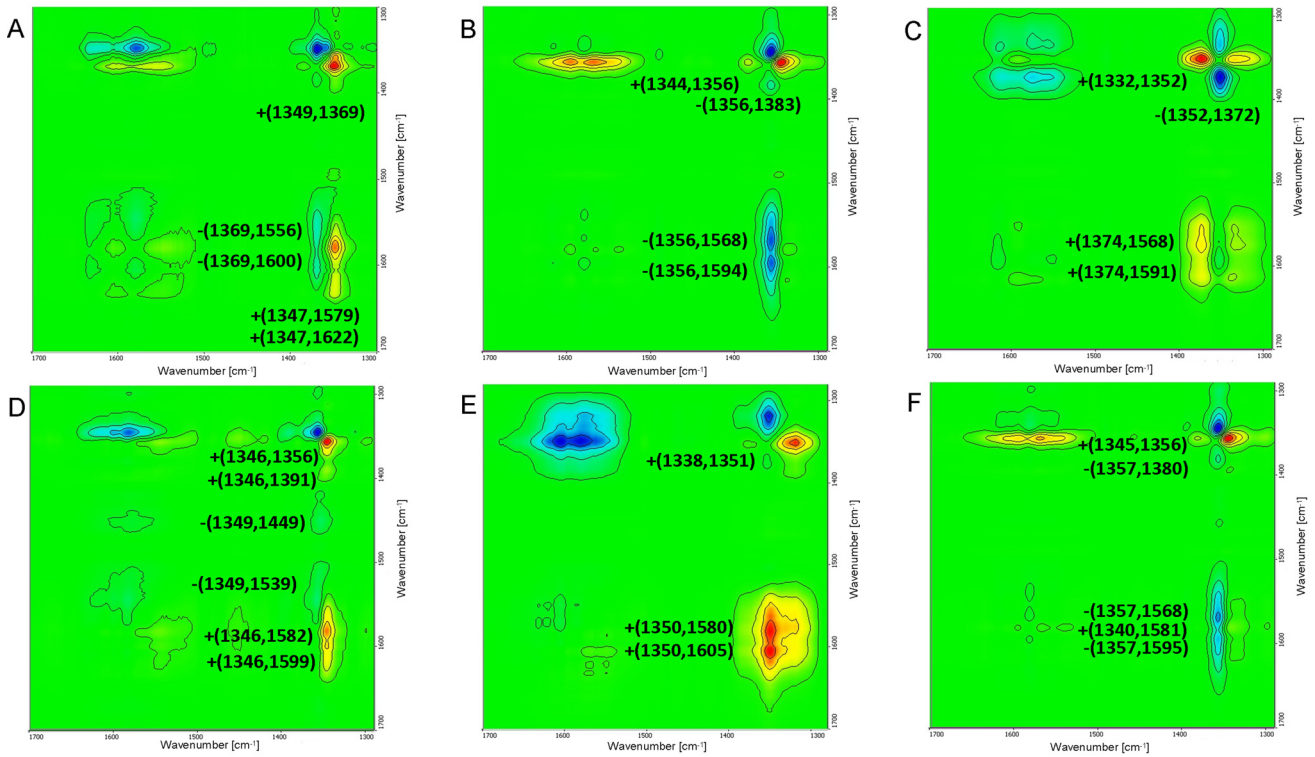

Fig. 4 2T2D asynchronous map discriminating healthy RBCs and with parasitemia malarial level: (A) 0.09%, (B) 0.14%, (C) 0.16%, (D) 1.17%, (E)7.45% and (F) 11.3%. Raman spectra obtained using 442 nm laser line.

position result from the sensitivity of vibrational spectra to small structural differences.[18] The results of the 2T2D analysis confirm that the intensity of a number of Raman bands is higher for the deoxy-heme structure than for the oxy-heme structure due to its absorption characteristics.[32]

Results obtained using 785 nm laser line

Synchronous 2D map obtained using a 785 nm laser line (see Fig. S2 and Fig. 5A) showed several distinct autopeaks, and one prominent cross-peak. The auto-peak at 976 cm^{-1} comes from the stretching modes of the protein and lipid backbones ν(C–C), in particular the stretching of phosphatidylcholine (PC),[28] as well as (ν_{46}) the asymmetric pyrrole deformation mode δ_{asym}(pyr. deform).[33] Changes in the PC vibrations seem to be related to the membrane fluidization process as a result of its invasion into the blood cell.[34] Another autopeak is located at 1004 cm^{-1}. This autopeak is generated by phenylalanine breathing mode (Phe), hemozoin stretching ν(Hz)[27] and (ν_{45}) heme stretching mode (ν(C_β=C_1)). Autopeak at 1234 cm^{-1} comes from tyrosine vibrations (Tyr) and (ν_{13}) heme

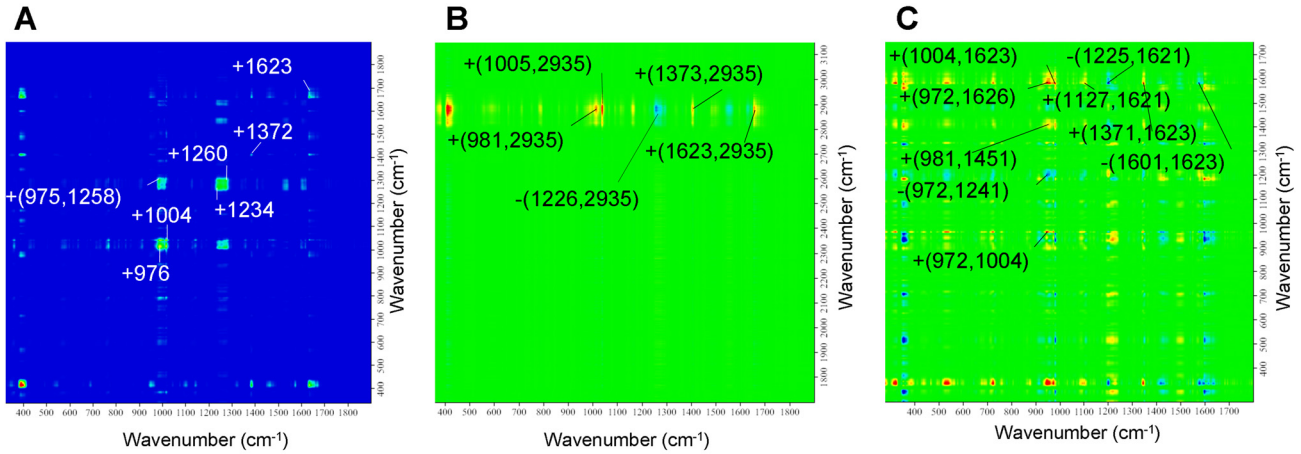

Fig. 5 2D map (*vide* Fig. S2) (A) synchronous in the spectral range 1900–300 cm^{-1}, and (B) asynchronous in the spectral range 1800–300 cm^{-1} *vs.* 3100–1900 cm^{-1}, and (C) asynchronous in the spectral range 1900–300 cm^{-1} obtained by correlating Raman spectra obtained using 785 nm laser line. The peaks of interest are labelled.

deformation mode ($\delta(C_m–H)$). Autopeak at 1260 cm^{-1} results from aspartic acid vibrations (Asp), glutamic acid vibrations (Glu), (ν_{42}) heme deformations ($\delta(C_m–H)$) and amide III vibrations of the α-helix structures.[28] The rather weak autopeak at 1372 cm^{-1} correspond to the symmetric (ν_4) vibrations of oxy-heme (ν_{sym}(pyr. half-ring)). The autopeak at 1623 cm^{-1} is due to the vibrations of tyrosine (Tyr), and tryptophan (Trp) and also heme stretching mode between C_a and C_b carbons ($\nu_{(C=C)}$). The relatively weak autopeak at 2927 cm^{-1} is made up of vibrations of proteins and lipids, symmetric and antisymmetric stretching vibrations of methyl and methylene groups $\nu_{sym}(CH_3)$ + $\nu_{asym}(CH_2)$, in particular vibrations of phosphatidylcholine vibrations (PC). Lastly, at 2938 cm^{-1} another autopeak can be seen, which consists of complex protein vibrations ($\nu_{sym}(CH_3)$ + $\nu_{asym}(CH_2)$) and phosphatidylethanolamine (PE) component of the internal lipid monolayer.[28] Changes in the PC and PE vibrations are related to the membrane fluidization process as a result of its development in the blood cell, which takes place outside and inside the monolayer.[33] The only prominent cross-peak is located at +(975, 1258) cm^{-1}. The band at 975 cm^{-1} comes from vibrations of proteins and lipids backbone ν(C–C) stretching modes, phosphatidylcholine stretching (PC), and (ν_{46}) antisymmetric pyrrole deformation mode (δ_{asym}(pyr. deform)). The band at 1258 cm^{-1} originated from tyrosine (Tyr), aspartic acid vibrations (Asp), glutamic acid vibrations (Glu), heme (ν_{42}) deformations between C_m carbons and hydrogens attached to it ($\delta(C_m–H)$) and amide III vibrations of the α-helix structures. The appearance of phosphatidylcholine may indicate the stage of parasite invasion and changes in the outer layer of the erythrocyte membrane.[11,33]

The appearing synchronous two-dimensional cross-peaks obtained for 785 nm excitation line illustrate the changes occurring in the structure of amino acids, proteins and lipids of the infected erythrocytes and are collected in Table 3.

Asynchronous 2D map obtained using 785 nm laser line displayed a number of different cross-peaks, both in the characteristic heme region, as well as in the lipid and protein region. Unlike 2D map obtained with 442 nm laser line, the asynchronous map obtained using 785 nm laser contains two separate regions of interest. These areas are shown in Fig. 5B and C.

Fig. 5C contains positive cross-peaks at +(972, 1004) and +(972, 1626) cm^{-1}. The band at 972 cm^{-1} indicates origin from proteins and lipids backbone stretching modes ν(C–C), phosphatidylcholine stretching (PC),[28] and (ν_{46}) asymmetric pyrrole deformation mode (δ_{asym}(pyr. deform)). Then, the band at 1004 cm^{-1} is made up of phenylalanine stretching mode vibrations (Phe), hemozoin stretching ν(Hz) and heme (ν_{45}) stretching mode ($\nu(C_\beta{=}C_1)$). The band at 1626 cm^{-1} is made up of tyrosine (Tyr), and tryptophan (Trp) vibrations[34] as well as heme stretching mode between C_a and C_b carbons ($\nu_{(C=C)}$). The 972 cm^{-1} vibration generates also a negative correlation peak at –(972, 1241) cm^{-1}. The band at 1241 cm^{-1} consists of aspartic acid vibrations (Asp), glutamic acid vibrations (Glu), heme (ν_{42}) deformations between C_m carbons and hydrogens attached to it ($\delta(C_m–H)$) and amide III vibrations of the α-helix structures. In many cross-peaks the signal from His appears, indicating possible HRP2 production.[34] The remaining amino acids indicate the metabolic activity of *Plasmodium*,[19] which precedes the changes occurring in the heme.

The cross-peak at +(981, 1451) cm^{-1} is made up of (ν_{46}) antisymmetric pyrrole deformation mode (δ_{asym}(pyr. deform)) for the band at 981 cm^{-1}, with histidine vibrations (His) and vinyl stretching modes ($\delta(=C_bH_2)$).

The cross-peak at +(1004, 1623) cm^{-1} consists of the vibrations of hemozoin (Hz) and phenylalanine (Phe) and (ν_{45}) stretching ($\nu(C_\beta{=}C_1)$) for the band at 1004 cm^{-1}. The band at 1623 cm^{-1} consists of tyrosine (Tyr) and tryptophan (Trp) vibrations. The cross-peak at –(1225, 1621) cm^{-1} consists of (ν_{13}) deformation vibrations ($\delta(C_m–H)$) for the band at

Table 3 The prominent synchronous and asynchronous cross-peaks and their assignments, 785 nm laser line[11,16–20,28,30,33]

Synchronous		Asynchronous		
Auto-peaks	Assignments	Assignments	Cross-peaks	Assignments
976	ν_{46}; δ_{asym}(pyr. deform); ν(C–C); PC; δ(=CH)	ν_{46}; δ_{asym}(pyr. deform); ν(C–C); PC	+(972, 1004)	ν_{45}; Phe; ν(Hz); $\nu(C_\beta{=}C_1)$
1004	ν_{45}; Phe; ν(Hz); $\nu(C_\beta{=}C_1)$		−(972, 1241)	ν_{42}; Amide $III_{(\alpha\text{-helix})}$; Asp; Glu; $\delta(C_m{-}H)$
1234	ν_{13}; Tyr; $\delta(C_m{-}H)$		+(972, 1626)	Tyr; Trp; His
1260	Amide $III_{(\alpha\text{-helix})}$; Asp; Glu; $\delta(C_m{-}H)$	ν_{46}; δ_{asym}(pyr. deform)	+(981, 1451)	His; $\delta(=C_bH_2)$
1372 weeks	ν_4; ν_{sym}(pyr. half-ring)$_{oxy}$, ν(Hz)		+(981, 2935)	$\nu_{sym}(CH_3) + \nu_{asym}(CH_2)$; PE
1623	Tyr; Trp	ν_{45}; Phe; ν(Hz); $\nu(C_\beta{=}C_1)$	+(1004, 1623)	Tyr; Trp
2927 weeks	$\nu_{sym}(CH_3) + \nu_{asym}(CH_2)$; PC; $\nu_{sym}(CH_3)_{lipid}$		+(1005, 2935)	$\nu_{sym}(CH_3) + \nu_{asym}(CH_2)$; PE
2938 weeks	$\nu_{sym}(CH_3) + \nu_{asym}(CH_2)$; proteins and lipids; PE	ν_{22}; ν_{asym}(pyr. half-ring)	+(1127, 1621)	Tyr; Trp
Assignments	Cross-peaks Assignments	ν_{13}; $\delta(C_m{-}H)$	−(1225, 1621)	
ν_{46}; δ_{asym}(pyr. deform); ν(C–C); PC	+(975, 1258) Amide $III_{(\alpha\text{-helix})}$; Trp		−(1226, 2935)	$\nu_{sym}(CH_3) + \nu_{asym}(CH_2)$; PE
		ν_4; ν_{sym}(pyr. half-ring)$_{oxy}$	+(1371, 1623)	Tyr; Trp
			+(1373, 2935)	$\nu_{sym}(CH_3) + \nu_{asym}(CH_2)$; PE
		ν_{19}; $\nu_{asym}(C_\alpha{=}C_m)$ Tyr; Trp	−(1601, 1623)	Tyr; Trp
			+(1623, 2935)	$\nu_{sym}(CH_3) + \nu_{asym}(CH_2)$; PE

Asp – aspartic acid, Glu – glutamic acid, His – histidine, Hz – hemozoin, Phe – phenylalanine, Thr – threonine, Trp – tryptophan, Tyr – tyrosine, PC – phosphatidylcholine, PE – phosphatidylethanolamine, w – weak.

1225 cm^{-1}, as well as tyrosine (Tyr) and tryptophan (Trp) vibrations for the band at 1621 cm^{-1}. The cross-peak at +(1127, 1621) cm^{-1} subsists of (ν_{22}) antisymmetric pyrrole half-ring stretching of heme (ν_{asym}(pyr. half-ring)) for the band at 1127 cm^{-1}, as well as tyrosine (Tyr) and tryptophan (Trp) vibrations for the band at 1621 cm^{-1}. The cross-peak at +(1371, 1623) cm^{-1} is made up of (ν_4) symmetric stretching of oxy-heme (ν_{sym}(pyr. half-ring)) for the band at 1371 cm^{-1} as well as tyrosine (Tyr) and tryptophan (Trp) vibrations for the band located at 1623 cm^{-1}. Lastly, the cross-peak at −(1601, 1623) cm^{-1} consists of (ν_{19}) antisymmetric vinyl stretching mode ($\nu_{asym}(C_\alpha{=}C_m)$) for the band at 1601 cm^{-1} as well as tyrosine (Tyr) and tryptophan (Trp) vibrations for 1623 cm^{-1}.

Fig. 5B contains cross-peaks, that all share the same band, located at 2935 cm^{-1}. This vibration is composed of protein skeleton stretching modes, symmetric for CH_3 and antisymmetric for CH_2 ($\nu_{sym}(CH_3) + \nu_{asym}(CH_2)$) and comes from phosphatidylethanolamine (PE), component of the inner lipid monolayer.[28] A series of vibrations correlate asynchronously with this mode. Firstly, the cross-peak at +(981, 2935) cm^{-1} consists of a band at 981 cm^{-1}, which indicates asymmetric pyrrole deformations in heme δ_{asym}(pyr. deform) (ν_{46}), and of band located at 2935 cm^{-1}. The next cross-peak is located at +(1005, 2935) cm^{-1}. The band at 1005 cm^{-1} consists of phenylalanine breathing mode (Phe), hemozoin vibrations (Hz) as well as (ν_{45}) a vinyl stretching mode ($\nu(C_\beta{=}C_1)$). Next, the peak at −(1226, 2935) cm^{-1} subsists of (ν_{13}) due to deformations between C_m carbons and the hydrogens attached ($\delta(C_m{-}H)$), which constitute the band at 1226 cm^{-1}. The next cross-peak is located at +(1373, 2935) cm^{-1}. The band at 1373 cm^{-1} indicates (ν_4) symmetric vibrations of oxy-heme (ν_{sym}(pyr. half-ring)). The last cross-peak of interest is located at +(1623, 2935) cm^{-1}. The band at 1623 cm^{-1} is made up of tyrosine (Tyr) and tryptophan (Trp) vibrations.

Changes in the oxy-heme structure asynchronous to changes in proteins and amino acids generate cross-peaks on the asynchronous map obtain for 785 nm excitation. Changes in the structure of oxy-heme correlate asynchronously with changes that are associated with PC, a phospholipid characteristic of the outer lipid layer.

All cross-peaks visible in the two-dimensional synchronous and asynchronous correlation maps generated using spectral data acquired with a 785 nm laser line are summarized in Table 3.

Conclusions

2D correlational maps obtained using 442 nm laser line show prominent, sharp cross-peaks, originating in the region heavily associated with heme vibrations, *i.e.* 1650 cm^{-1}–650 cm^{-1}. The synchronous 2D map displays only positive cross-peaks, which means that the changes in the studied system, which are characterized by the intensities of the corresponding bands, have the same character. Most cross-peaks are generated by vibrations of hemozoin, an aggregated form of heme produced as a result of *Plasmodium* activity. The asynchronous 2D map shows both positive and negative peaks, indicating a phase change between some peaks, occurring in the sequence of increasing disturbance, which is parasitemia. Asynchronous cross-peaks usually come from deoxy- and oxy-heme structures, emphasizing the differences between them, their dissimilarity. Different positions of cross-peaks originating from

the ν_4 heme vibrations, show specific heme intermediates depending on the external disturbance which is parasitemia.

2D maps created by correlating spectra collected with 785 nm laser show a wide range of peaks. These peaks are consisting of bands visible due to vibrations specific to heme, proteins, lipids of human and *Plasmodium* origin. Synchronous 2D map displays multiple autopeaks with one prominent, positive cross-peak at +(975, 1258), that reflects changes in heme vibrations that lead to changes in amide III of perhaps a parasitic protein.[33]

For the 785 nm excitation wavelength, changes in the oxy-heme structure correlates asynchronously with changes in proteins and amino acids and generate cross peaks on the two-dimensional asynchronous map.

Changes in the oxy-heme forms (ν_4) but also in the aggregated heme forms (ν_{46}, ν_{45}, ν_{13}) precede changes in PE characterizing the inner layer of the biological membrane.

To conclude, Raman spectroscopy combined with 2D correlational spectroscopy was able to highlight the correlation between different changes in erythrocytes, occurring as a result of *P. falciparum* infection. This topic requires further study, to ascertain the degree, to which this method may be used as a viable and reliable tool in detecting malaria-induced changes to the erythrocytes, as well as to widen its possible applicability in regard to different strains of *Plasmodium* parasites.

Conflicts of interest

There are no conflicts to declare.

Data availability

All data generated or analyzed during this study are included in this published article. The data used and/or analyzed during the current study are available from the corresponding author upon reasonable request.

Supplementary information (SI) is available. See DOI: https://doi.org/10.1039/d5an00272a.

Acknowledgements

This study was supported by the subsidiary research part of Jagiellonian Universities Faculty of Chemistry, Kraków, Poland. M. M. acknowledges support from ID. UJ (from the Faculty of Chemistry under the Strategic Programme Excellence Initiative at Jagiellonian University) funds.

References

1 World Health Organization, *World malaria report 2023*, Geneva, 2023, pp. XVII–XXXV.
2 World Health Organization, Malaria, https://www.who.int/news-room/fact-sheets/detail/malaria (accessed September 8, 2024).
3 Centers for Disease Control and Prevention, Symptoms of Malaria, https://www.cdc.gov/malaria/symptoms/index.html (accessed September 8, 2024).
4 World Health Organization, How malaria RDTs work, https://www.who.int/teams/global-malaria-programme/case-management/diagnosis/rapid-diagnostic-tests/how-malaria-rdts-work (accessed September 8, 2024).
5 H. Noedl, W. H. Wernsdorfer and R. S. Miller, Histidine-Rich Protein II: a Novel Approach to Malaria Drug Sensitivity Testing, *Antimicrob Agents Chemother*, 2002, **46**, 1658, DOI: 10.1128/2FAAC.46.6.1658-1664.2002.
6 M. Migdalski, J. Czepiel, P. Moskal, M. Birczyńska-Zych, M. Kucharska, G. Biesiada, A. Stokłosa, A. Garlicki and A. Wesełucha-Birczyńska, Raman and resonance Raman spectroscopic study of red blood cells in patients diagnosed with malaria, *Spectrochim. Acta, Part A*, 2025, **325**, 125037, DOI: 10.1016/j.saa.2024.125037.
7 A. Wesełucha-Birczyńska, M. Kozicki, J. Czepiel, M. Łabanowska, P. Nowak, G. Kowalczyk, M. Kurdziel, M. Birczyńska, G. Biesiada, T. Mach and A. Garlicki, Human erythrocytes analyzed by generalized 2D Raman correlation spectroscopy, *J. Mol. Struct.*, 2014, 305–312, DOI: 10.1016/j.molstruc.2014.03.023.
8 M. Kozicki, J. Czepiel, G. Biesiada, P. Nowak, A. Garlicki and A. Wesełucha-Birczyńska, The ring-stage of Plasmodium falciparum observed in RBCs malaria hospitalized patients, *Analyst*, 2015, **140**, 8007–8016, DOI: 10.1039/C5AN01598G.
9 M. Birczyńska-Zych, J. Czepiel, M. Łabanowska, M. Kraińska, G. Biesiada, P. Moskal, M. Kozicki, A. Garlicki and A. Wesełucha-Birczyńska, Could Raman spectroscopy distinguish between *P. falciparum* and *P. vivax* infection?, *Clin. Spectrosc.*, 2021, **3**, **100015**, 1–10, DOI: 10.1016/j.clispe.2021.100015.
10 M. Birczyńska-Zych, J. Czepiel, M. Łabanowska, M. Kurdziel, G. Biesiada, M. Kozicki, A. Garlicki and A. Weselucha-Birczynska, The aging of *P. falciparum* infected RBCs by 2D-correlation Raman and EPR Spectroscopy, *J. Mol. Struct.*, 2021, **1224**(1–12), 129036, DOI: 10.1016/j.molstruc.2020.129036.
11 M. Birczyńska-Zych, J. Czepiel, M. Łabanowska, M. Kucharska, M. Kurdziel, G. Biesiada, A. Garlicki and A. Wesełucha-Birczyńska, Course of *Plasmodiu*m, infection studied using 2D-COS on human erythrocytes, *Malaria J.*, 2023, **22**, 188, DOI: 10.1186/s12936-023-04611-5.
12 I. Noda, Generalized Two-Dimensional Correlation Method Applicable to Infrared, Raman, and Other Types of Spectroscopy, *Appl. Spectrosc.*, 1993, **47**, 1329–1336, DOI: 10.1366/0003702934067694.
13 I. Noda, A. E. Dowrey, C. Marcott, G. M. Story and Y. Ozaki, Generalized Two-Dimensional Correlation Spectroscopy, *Appl. Spectrosc.*, 2000, **54**, 236A–241A, DOI: 10.1366/0003702001950454.

14 Y. Park, I. Noda and Y. M. Jung, Two-dimensional correlation spectroscopy in polymer study, *Front. Chem.*, 2015, **3**, 14, DOI: 10.3389/fchem.2015.00014.
15 I. Noda, Two-Dimensional Infrared (2D IR) Spectroscopy: Theory and Applications, *Appl. Spectrosc.*, 1990, **44**(4), 550–561.
16 T. G. Spiro, Resonance Raman Spectroscopy as a Probe of Heme Protein Structure and Dynamics, C.B. Anfinsen, J. T. Edsall, F.M. Richards, *Adv. Protein Chem.*, 1985, **37**, 111–159, DOI: 10.1016/S0065-3233(08)60064-9.
17 T. Kitagawa and Y. Ozaki, Infrared and Raman spectra of metalloporphyrins, in *Metal Complexes with Tetrapyrrole Ligands I*, ed. J. W. Buchler, Springer-Verlag, 1987, pp. 71–114, DOI: 10.1007/BFb0036790.
18 I. Salmeen, L. Rimai, D. Gill, T. Yamamoto, G. Palmer, C. R. Hartzell and H. Beinert, Resonance Raman Spectroscopy of Cytochrome 2 Oxidase and Electron Transport Particles with Excitation near the Soret Band, *Biochem. Biophys. Res. Commun.*, 1973, **52**, 1100–1107, DOI: 10.1016/0006-291x(73)91051-6.
19 M. Kozicki, D. J. Creek, A. Sexton, B. J. Morahan, A. Wesełucha-Birczyńska and B. R. Wood, An attenuated total reflection (ATR) and Raman spectroscopic investigation into the effects of chloroquine on *Plasmodium falciparum*-infected red blood cells, *Analyst*, 2015, **140**, 2236, DOI: 10.1039/C4AN01904K.
20 B. R. Wood and D. McNaughton, Raman excitation wavelength investigation of single red blood cells *in vivo*, *J. Raman Spectrosc.*, 2002, **33**, 517–523, DOI: 10.1002/jrs.870.
21 J. Lin, J. Lin, Z. Huang, P. Lu, J. Wang, X. Wang and R. Chen, Raman Spectroscopy of Human Hemoglobin for Diabetes Detection, *J. Innov. Opt. Health Sci.*, 2014, **7**(1), 1350051, DOI: 10.1142/S179354581350051X.
22 S. Kumar, V. Kumar and D. C. Jain, Laser Raman Spectroscopic Studies on Hemeproteins in Epileptic Children, *Open J. Appl. Sci.*, 2013, **3**(1), 123–135, DOI: 10.4236/ojapps.2013.31018.
23 J. Czepiel, M. Kozicki, P. Panasiuk, M. Birczyńska, A. Garlicki and A. Wesełucha-Birczyńska, Clostridium difficile the hospital plague, *Analyst*, 2015, **140**, 2513–2522, DOI: 10.1039/C4AN01947D.
24 A. Kurek, P. Moskal, J. Czepiel, M. Birczyńska-Zych, M. Bociąga-Jasik and A. Wesełucha-Birczyńska, Analysis of red blood cells from individuals with allergy symptoms using Raman spectroscopy, *J. Mol. Struct.*, 2025, DOI: 10.2139/ssrn.5200455, in review.
25 S. Hu, K. M. Smith and T. G. Spiro, Assignment of Protoheme Resonance Raman Spectrum by Heme Labeling in Myoglobin, *J. Am. Chem. Soc.*, 1998, **118**, 12638–12646, DOI: 10.1021/ja962239e.
26 M. Abe, T. Kitagawa and Y. Kyogoku, Resonance Raman spectra of octaethylporphyrinato-Ni(II) and meso -deuterated and 15N substituted derivatives. II. A normal coordinate analysis, *J. Chem. Phys.*, 1978, **69**, 4526–4534, DOI: 10.1063/1.436450.
27 D. McNaughton and B. R. Wood, Resonance Raman spectroscopy in malaria research, *Expert Rev. Proteomics*, 2006, **3**, 525–544, DOI: 10.1586/14789450.3.5.525.
28 A. T. Tu, *Raman spectroscopy in biology: principles and applications*, *Wiley*, 1982.
29 B. Knapp, E. Hundt and K. R. Lingelbach, Structure and possible function of Plasmodium falciparum proteins exported to the erythrocyte membrane, *Parasitol. Res.*, 1991, **77**, 277–282, DOI: 10.1007/BF00930901.
30 H. Takeuchi, Raman structural markers of tryptophan and histidine side chains in proteins, *Biopolymers*, 2003, **72**, 305–317, DOI: 10.1002/bip.10440.
31 I. Noda, Two-trace two-dimensional (2T2D) correlation spectroscopy – A method for extracting useful information from a pair of spectra, *J. Mol. Struct.*, 2018, **1160**, 471–478, DOI: 10.1016/j.molstruc.2018.01.091.
32 H. Brunner, A. Mayer and H. Sussner, Resonance Raman scattering on the haem group of oxy- and deoxyhaemoglobin, *J. Mol. Biol.*, 1972, **70**, 153–156, DOI: 10.1016/0022-2836(72)90169-6.
33 B. R. Wood, P. Caspers and G. J. Puppels, Resonance Raman spectroscopy of red blood cells using near-infrared laser excitation, *Anal. Bioanal. Chem.*, 2007, **387**, 1697–1703, DOI: 10.1007/s00216-006-0881-8.
34 L. L. Hsiao, R. J. Howard, T. Aikawa and F. Taraschi, Modification of host cell membrane lipid composition by the intra-erythrocytic human malaria parasite *Plasmodium falciparum*, *Biochem. J.*, 1991, **274**, 121–132, DOI: 10.1042/bj2740121.